

Si–N linkage in ultrabright, ultrasmall Si nanoparticles

E. Rogozhina

*Department of Material Science and Engineering and Beckman Institute for Science and Technology,
University of Illinois at Urbana–Champaign, Urbana, Illinois 61801*

G. Belomoin and A. Smith

Department of Physics, University of Illinois at Urbana–Champaign, Urbana, Illinois 61801

L. Abuhassan

Physics Department, University of Jordan, Amman, Jordan

N. Barry and O. Akcakir

Department of Physics, University of Illinois at Urbana–Champaign, Urbana, Illinois 61801

P. V. Braun

*Department of Material Science and Engineering and Beckman Institute for Science and Technology,
University of Illinois at Urbana–Champaign, Urbana, Illinois 61801*

M. H. Nayfeh^{a)}

Department of Physics, University of Illinois at Urbana–Champaign, Urbana, Illinois 61801

(Received 30 January 2001; accepted for publication 12 April 2001)

Ultrabright ultrasmall (~ 1 nm) blue luminescent Si₂₉ nanoparticles are chlorinated by reaction with Cl₂ gas. A Si–N linkage is formed by the reaction of the chlorinated particles with the functional amine group in butylamine. Fourier transform infrared spectroscopy and x-ray photospectroscopy measurements confirm the N linkage and the presence of the butyl group, while emission, excitation, and autocorrelation femtosecond optical spectroscopy show that, after the linkage formation, the particles with the ultrabright blue luminescent remain, but with a redshift of 40 nm. © 2001 American Institute of Physics. [DOI: 10.1063/1.1377619]

We recently developed a class of Si-based detection,^{1–6} with significant potential, as the next generation of ultrabright nonorganic markers for ultrasensitive fluorescence analysis. We dispersed bulk Si into nanoparticles of uniform size of ~ 1 nm diam (Si₂₉).⁷ This miniaturization effectively creates a nanoparticle material with properties—both electronic and nonelectronic—that were not available before. These include ultrabright luminescence such that emission from single particles is readily detectable,^{2,3} stimulated emission,¹ collimated emission beams,⁵ and second-harmonic generation⁶ from films of the particles. Most importantly, the particles are photostable and do not blink. Present-day medical and biological fluorescent imaging is significantly constrained by the use of dye markers—the only markers currently available.⁸ Dyes, especially the blue ones, are not photostable—they decompose under room light or higher temperatures. Efforts are being directed to produce different classes of markers, such as semiconductor particles. CdS (e) nanoparticles have recently been proposed as fluorescent markers.^{9,10} Implementation of Si-based detection will require routes to couple biopolymers to the surface of the silicon nanoparticles via a covalent linkage. Here, we present a step toward this goal, the covalent linking of a model organic compound to the surface of the particles. We demonstrate the formation of an organic hydrophobic shell due to the attachment of butylamine while still maintaining the optical activity of the particle. The particles were chlorinated by reaction with Cl₂ gas, followed by the reaction with

the functional amine group in butylamine to form a Si–N linkage. The linkage facilitates the attachment of organic functional groups capable of recognizing specific analytes such as proteins, DNA, or viruses. The exceptional optical properties, ultrasmall size (\sim small molecules), uniformity of size, low cost, and photostability provide the ultimate sensitivity and spatial resolution in imaging capabilities.

The synthesis of the Si particles has been described elsewhere.^{1–7} Briefly, we used highly catalyzed electrochemical etching to disperse crystalline Si into ultrasmall nanoparticles. The substrates were (100)-oriented, 1–10 Ω cm resistivity, *p*-type, B-doped Si, laterally anodized in hydrogen peroxide and HF,^{11,12} while advancing the wafer at a slow speed. Subsequent immersion in an ultrasound bath of chlorobenzene crumbles the top film into ultrasmall particles. When it is excited by radiation at 355 nm, deep blue emission is observed with the naked eye. Direct imaging, using transmission electron microscopy, of a graphite grid coated with the particles gives a diameter of 1 nm with 10% dispersion.² Electron photospectroscopy and infrared Fourier spectroscopy show that the particles are composed of silicon, dominated by hydrogen termination with less than 10% oxygen.

Porous Si layers^{13,14} and nanoparticles¹⁵ have been recently functionalized through a number of processes. The aminization in our work follows a recent procedure used to aminize flat as well as porous-Si surfaces.¹⁶ The chlorobenzene colloid of particles is first degassed and then saturated with Cl₂ gas at a temperature of -10 °C. The reaction mixture is then stirred for 24 h at room temperature.¹⁶ The dis-

^{a)}Electronic mail: m-nayfeh@uiuc.edu

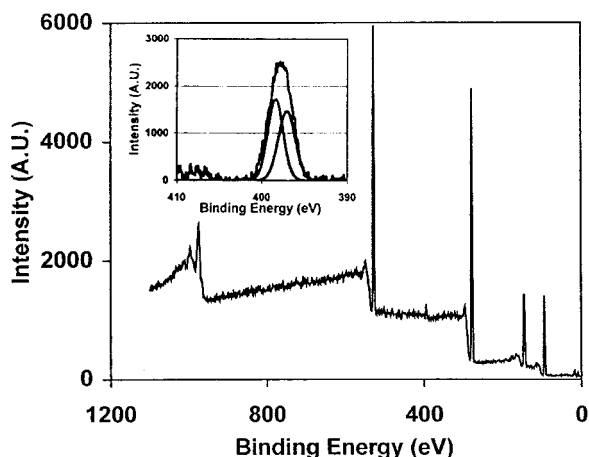


FIG. 1. XPS spectra of films reconstituted from the particles showing that the aminized particles have nitrogen and carbon peaks at ~ 400 and 300 eV, respectively. A fit of the binding energy of the 400 eV peak in terms of two components is given in the inset.

solved chlorine gas chlorinates the particles, replacing the hydrogen with chlorine. The excess dissolved Cl_2 , HCl by-product and the solvent are removed by evaporation. Freshly distilled butylamine ($\text{C}_4\text{H}_9\text{NH}_2$) is then added to the dried sample. The solution is heated to 90°C and stirred for 24 h at that temperature. The excess butylamine is then evaporated and the dried particles are dissolved in heptane. Several drops of the colloid are placed on a Si substrate. After drying in air or under nitrogen, a few-micron-thick particle film forms.

Figure 1 presents the x-ray photospectra (XPS) of a film of aminized particles. Both the N and C peaks at ~ 400 and 300 eV, respectively, are observed. The best fit of the 400 eV peak, shown in the inset, gives two components at 397.120 and 398.436 eV with 1.762 and 1.875 full width at half maximum and 43.9 and 56.1 percentage mass concentration, respectively. These are associated with the N $1s$ of bulk Si nitride, and amine molecules (typically, at 399 eV), respectively. The low-energy one is consistent with well-established surface chemistry in the absorption of NH_3 on Si surfaces and in the atomic layer growth of Si_3N_4 .¹⁷ These lend support for binding through a Si–N linkage. Further confirmation is derived from the Fourier transform infrared (FTIR) spectra given in Fig. 2. The aminized samples show a strong N–H stretch at ~ 3300 cm^{-1} , and a Si–N stretching mode at 860 cm^{-1} . The peaks at 2869 , 2881 , 2931 , and 2966 cm^{-1} are characteristics of C–H stretch vibrations in butyl groups. The vibrations at ~ 2300 and 1000 – 1100 pertain to

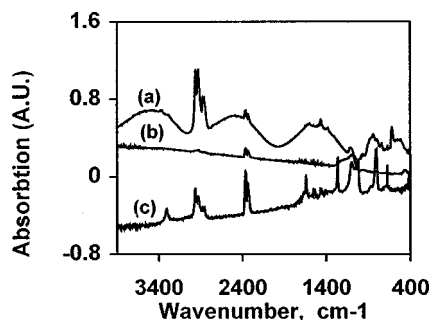


FIG. 2. Fourier transform infrared (FTIR) spectra of (a) butylamine, (b) bare Si substrate, and (c) aminized particles cast on the substrate.

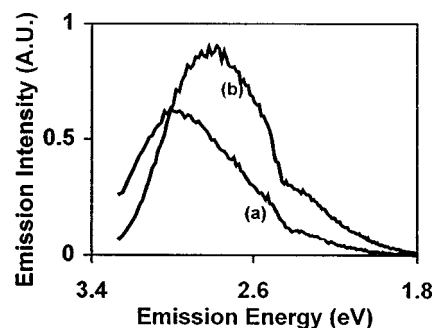


FIG. 3. Unnormalized emission spectra of the dispersed particles at 365 nm: (a) before and (b) after the aminization.

CO_2 air and oxygen. The peaks at 1460 and 1260 are due to CH_2 – CH_3 stretching and CH_2 wagging, respectively. The 1450 – 1700 band is the background seen also in the control samples. XPS taken after air exposure did not show a significant change in the N $1s$. The presence of the H–N bond is a strong indication of single Si–N formation as opposed to a bridge double-bond-linkage Si–N–Si. Aminization of Si flat or porous surfaces using a similar chemical treatment showed preference to the bridge formation. In these systems, XPS showed nitrogen bonds but FTIR showed the absence of the N–H vibration.¹⁶

The emission was recorded on a photon-counting spectrofluorometer with a Xe arc lamp light source and 4 nm bandpass excitation and emission monochrometers, with suitable filtering and correction for spectral response. The detector has a cutoff at 950 nm. Figure 3 gives the emission spectrum of the dispersed particles at 365 nm before and after aminization. In both cases, the spectrum is dominated by a strong blue band with a tail band that extends into the visible, diminishing at ~ 600 nm. The peak of the blue band of the hydrogenated particle shifts from 410 to 450 nm upon aminization.

Figure 4 gives the emission of the aminized particles and its development with the incident wavelength. As the incident wavelength is increased from 330 nm, the blue band peaks at 410 (not shown), 440 , 475 , and 540 nm for 330 , 365 , 400 , and 470 nm incident wavelengths, respectively, i.e., the peak of the emission energy correlated with the excitation photon energy. Second, with increasing incident wavelength, the strength of the emission tail band grows relative to the main blue band, and the overall efficiency maximizes for 400 nm excitation. The emission is very strong such that when the colloid is excited by 400 nm ra-

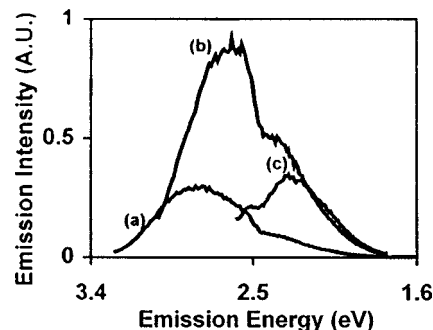


FIG. 4. Relative emission of the aminized particles and its development with the incident wavelength, (a) 365 nm, (b) 400 nm, and (c) 470 nm.

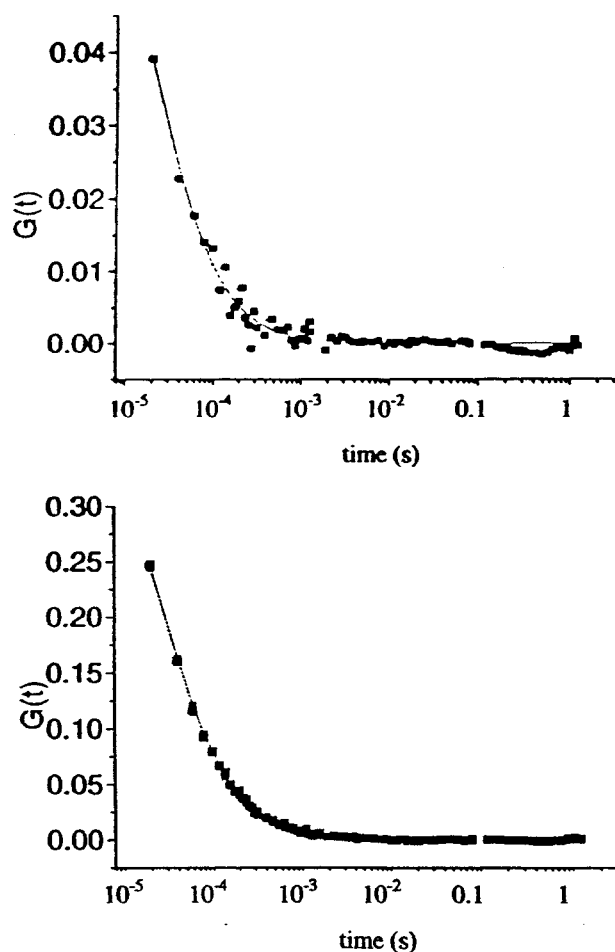


FIG. 5. Autocorrelation function G as a function of time derived from the emission of (top) the particles in a colloid along with that of (bottom) a coumarine standard under two-photon excitation using mode-locked near infrared. The functions belong to one particle and 0.2 molecules in the focal volume.

diation (30 ns pulses), the blue emission is observable with the naked eye, in room light.

We used two-photon excitation (780 nm, 150 fs duration at 80 MHz). At the target, the average power, 20 mW, is focused to a spot of $0.8 \mu\text{m}$ diam. The beam-sample interaction is viewed via an optical microscope ($\times 20$). Emission is detected by a photomultiplier or by an avalanche photodiode (20% efficiency). We used this process to determine the particle's brightness by autocorrelation fluctuation spectroscopy.³ The raw traces of emission are recorded. Figure 5 gives the autocorrelation function $\int_a I(t+\tau)I(t)^* dt$ of a very diluted particle sample along with a diluted coumarine dye where I is the emission intensity. The functions are fitted to a Gaussian diffusion function: $A [1/(1+8Dt/w^2)] \times SQRT[1/(1+8Dt/z^2)] + B$, where w is the waist of the beam, z is the depth of the focal volume, t is in millisecond, D is the diffusion coefficient, B is an offset, $A = 0.076/N$ is the $t=0$ intercept, N is the number of aminized particles in

the focal volume, and 0.076 is a calibration factor from a standard coumarine measurement (known density and diffusion coefficient), taken under the same beam focusing. The results yield $w = 400 \text{ nm}$ and $z = 1.98 \mu\text{m}$, or a volume of 0.997 picocubic centimeters, and $N = 1$ particle. This corresponds to a density of $3.45\text{--}3.85 \times 10^{12}/\text{cm}^2$. A similar analysis yields 0.2 coumarine molecules in the focal volume. From the photon-counting histograms (not shown), we find a brightness for the aminized particles twofold smaller than that of coumarine.

In conclusion, ultrabright, ultras-small ($\sim 1 \text{ nm}$) blue luminescent Si nanoparticles have been derivitized by termination with butylamine. This reaction is sufficiently general for the assembly of a variety of functional organic molecules on the particles. We demonstrated that the exceptional brightness of the nanoparticles are maintained after derivitization.

The authors acknowledge State of Illinois IDCCA Grant No. 00-49106, U.S. DOE Grant No. DEFG02-ER9645439, NIH Grant No. RR03155, Motorola, and the University of Illinois at Urbana-Champaign.

¹M. Nayfeh, O. Akcakir, J. Therrien, Z. Yamani, N. Barry, W. Yu, and E. Gratton, *Appl. Phys. Lett.* **75**, 4112 (1999).

²G. Belomoin, J. Therrien, and M. Nayfeh, *Appl. Phys. Lett.* **77**, 779 (2000).

³O. Akcakir, J. Therrien, G. Belomoin, N. Barry, E. Gratton, and M. Nayfeh, *Appl. Phys. Lett.* **76**, 1857 (2000).

⁴J. Therrien, G. Belomoin, and M. Nayfeh, *Appl. Phys. Lett.* **77**, 1668 (2000).

⁵M. Nayfeh, N. Barry, J. Therrien, O. Akcakir, E. Gratton, and G. Belomoin, *Appl. Phys. Lett.* **78**, 1131 (2001).

⁶M. Nayfeh, N. Barry, O. Akcakir, and G. Belomoin, *Appl. Phys. Lett.* **77**, 4086 (2000).

⁷L. Mitas, J. Therrien, R. Twesten, and M. H. Nayfeh, *Appl. Phys. Lett.* **78**, 1918 (2001).

⁸See, for example, *Immunoassays*, edited by E. P. Diamandis and T. K. Christopoulos (Academic, New York, 1996); *Protocols for Nucleic Acid Analysis by Nonradioactive Probes*, edited by P. G. Issac (Humana, Totowa, NJ, 1994); *Nonisotropic Probing, Blotting, and Sequencing*, edited by L. J. Kricka (Academic, New York, 1995).

⁹M. Bruchez, Jr., M. Moronne, P. Gin, S. Weiss, and A. P. Alivisatos, *Science* **281**, 2013 (1998).

¹⁰W. C. W. Chan and S. Nie, *Science* **281**, 2016 (1998).

¹¹Z. Yamani, H. Thompson, L. Abuhassan, and M. H. Nayfeh, *Appl. Phys. Lett.* **70**, 3404 (1997); D. Andsager, J. Hilliard, J. M. Hetrick, L. Abuhassan, M. Plisch, and M. H. Nayfeh, *J. Appl. Phys.* **74**, 4783 (1993).

¹²Z. Yamani, S. Ashhab, A. Nayfeh, and M. H. Nayfeh, *J. Appl. Phys.* **83**, 3929 (1998).

¹³M. J. Sailor and E. J. Lee, *Adv. Mater.* **9**, 783 (1997).

¹⁴M. R. Linford, P. Fenter, P. M. Eisenberger, and C. E. Chidsey, *J. Am. Chem. Soc.* **117**, 3145 (1995); N. Y. Kim and P. E. Laibinis, *ibid.* **119**, 2297 (1997); R. C. Anderson, R. C. Muller, and C. W. Tobias, *J. Electrochem. Soc.* **140**, 1393 (1993); A. Banasal, X. Li, I. Lauremann, N. S. Lewis, S. I. Yi, and W. H. Weinberg, *J. Am. Chem. Soc.* **118**, 7225 (1996); C. Viellard, M. Wartjes, F. Oznam, and J. N. Chazalviel, *Proc. Electrochem. Soc.* **95**, 250 (1996); J. H. Song and M. J. Sailor, *J. Am. Chem. Soc.* **120**, 2376 (1998).

¹⁵B. Sweryda-Krawiec, T. Cassagneau, and J. Fendler, *J. Phys. Chem. B* **103**, 9524 (1999).

¹⁶W. Bergerson, J. Mulder, R. Hsung, and X.-Y. Zhu, *J. Am. Chem. Soc.* **121**, 454 (1999); A. Taylor and B. de G. Walden, *ibid.* **66**, 842 (1944).

¹⁷S. George, A. Otto, and J. Kaus, *J. Phys. Chem.* **100**, 13121 (1996).